Incipient Fault Detection in Stator Windings of an Induction Motor Using Stockwell Transform and SVM

Megha Singh, *Student Member, IEEE*, and Abdul Gafoor Shaik

***Abstract*— In this article, Stockwell transform (ST) is used to analyze the stator current signals for diagnosis of various motor conditions such as healthy, stator winding interturn shorts, and phase to ground faults. ST decomposes the current signals into complex ST matrix whose magnitude has been utilized for the fault detection. The nature of the fault, that is, ground or interturn is identified using the zero sequence currents followed by postfault detection. Two separate frequency bands are defined to extract the features which are fed to two different support vector machine (SVM) models for faulty phase detection for both types of faults. Under both cases, a heuristic feature selection approach is utilized to find the optimal features for classification purposes. Average classification accuracy of 96% has been achieved for both types of faults.**

***Index Terms*— Stator fault diagnosis, Stockwell transform (ST), support vector machine (SVM), three phase induction motor (IM).**

I. Introduction

ONE of the main causes of the induction motor (IM) breakdown is the failure of insulation in the stator windings. In the presence of insulation failure, the faults in the stator can grow to serious faults hazardous to the motor. Such faults share about 30%–40% of the total motor faults [1], [2]. According to Grubic *et al*. [3] and Siddique *et al.* [4], they are generally caused due to a combination of vibrations caused by electromechanical forces, frequent motor start-ups and stops, high *dv*/*dt* voltage surges, mechanical stresses, thermal overload, and contamination. Insulation failure has a deteriorating and rapidly propagating tendency. It gradually starts as turn to turn shorts, causing a large short circuit current to flow in the windings leading to localized thermal overloading. Eventually, under continuous motor operation, it leads to shorting in the same or adjacent coils, phase to phase or ground faults. Thus, turn-to-turn shorts are a major source of deterioration of stator windings that culminates into wide range of faults such as 1) coil-to-coil fault, (2) phase-to-phase fault, and (3) coil-to-ground fault that may turn severe leading to catastrophic failure of the motor.

The long persistence of local shorting of turns may lead to severe faults that can burn off the motor winding in no time. Thus, monitoring of stator winding interturn shorts at an early stage of inception is of prime importance. For high-voltage motors up to 4 kV, partial discharge-based methods are utilized for stator-related faults. However, for low-voltage motors, fault detection methods are still in the process of finalization [5]. Nevertheless, in general, there is some lead time between turn-shorts to complete failure in the case of low-voltage motors [6]. This lead time is sufficient enough for diagnostic techniques to detect shorting of turns in the motor.

Several techniques based on the current signals are reported in [3], where the analysis is performed with negative sequence components, spectral analysis, high-resolution spectral analysis, Park/Concordia methods, high-frequency signal injection method, time-frequency analysis, and so on. A vast number of diagnostic approaches based on sequence components of the motor's current, impedance, and voltage have been reported in the literature. An approach based on negative sequence currents and voltages for interturn fault impedance is presented in [7] compensating the effects of voltage unbalance, inherent asymmetry to detect the early fault, identify the faulty phase, and provide an estimate of the fault severity level. In [8], features of Park's vector (PV) modulus using extended PV analysis in time, frequency, and time–frequency domain are extracted and nonlinear detrended fluctuation analysis is performed whose features are fed to support vector regression for interturn faults classification. Forward and backward currents with the help of Clarke transformation are computed and analyzed for turn-faults in [9].

High-resolution spectral analysis-based techniques such as multiple signal classification (MUSIC) and root-MUSIC have also been used for stator fault diagnosis [10]. The high-frequency properties of the transient current signals obtained after voltage excitation through switching of the inverter have been reported in [11] to be useful for stator interturn shorts detection. Negative sequence component-based methods suffer limitations in the presence of unbalanced voltages and load variations. High-frequency estimators though accurate in frequency estimation take high-computational complexity to run the algorithms. There are techniques that make use of time–frequency-based analysis for winding fault analysis, for example, short-time Fourier transform (STFT), wavelet transform (WT), and Wigner–Ville decomposition.

II. Related Work

The multiresolution capability of the WT and its extensions such as wavelet packet decomposition has been exploited in

Manuscript received January 7, 2020; revised May 25, 2020; accepted May 30, 2020. Date of publication June 15, 2020; date of current version November 10, 2020. The Associate Editor coordinating the review process was Tarikul Islam. *(Corresponding author: Megha Singh.)*

The authors are with the Department of Electrical Engineering, Indian Institute of Technology Jodhpur, Jodhpur 342037, India (e-mail: pg201384008@iitj.ac.in, saadgafoor@iitj.ac.in).

Color versions of one or more of the figures in this article are available online at http://ieeexplore.ieee.org.

Digital Object Identifier 10.1109/TIM.2020.3002444

the analysis of current signals for stator fault diagnosis [12]. The application of discrete and stationary WT is used to denoise and decompose the reconstructed current signals into detail coefficients for winding faults [13]. Seshadrinath *et al.* [14] proposed the use of dual-tree complex WT to decompose and reconstruct the current signals for 13 levels where their computed energies are fed to support vector machine (SVM) to classify stator winding faults. In [15] and [16], the energy is fed to a probabilistic neural network (NN) and SVM for the classification of healthy and interturn shorts under voltage unbalance and balance conditions. The application of discrete harmonic WT for fault diagnosis has been proposed by Sapena-Bañó. [17], which implements fast Fourier transform (FFT) and inverse FFT providing a low-cost solution for the fault diagnosis.

The widespread use of machine learning (ML) techniques for stator fault diagnosis has been reported in various articles [18], [19]. In [20], the use of artificial NN (ANN) and Kohonen self-organizing map (SOM) using statistical features of current signals under turn-shorts has been reported. Ballal *et al.* [22] used ANN and SOM along with the use of principal component analysis (PCA) to indicate the efficacy of feature reduction. The use of an adaptive neural fuzzy system is proposed with the machine parameters such as temperature, current, speed, and so on in [22]. A technique based on time series obtained using SOM-based fuzzy clustering is proposed [23], which is further analyzed for change point detection using the Metropolis–Hastings algorithm. Devi *et al.* [13] and Ali *et al*. [25] employed WT with a three-level modular NN to classify various levels of turn-shorts in the three-phase IM. The features from the matching pursuit and discrete WT of current and vibration signals are fed to 17 classifiers to compare their performances in [25]. In other application of SOM, the features selected from relief, minimum redundancy and maximum relevancy based on the features extracted from PV, and zero-crossing instants of current signals are used for clustering stator winding faults [26]. In [27] and [28], the mutual information of three-phase stator currents is fed to decision tree and ANN for the classification of interturn shorts. A variant of WT, Stockwell transform (ST), has also been used for motor fault diagnosis in [30] and [31].

Some articles reported techniques for interturn fault detection, while some other focused on ground fault detection. There is a need to propose a unique algorithm for these winding faults with less computational complexity and time. Hence, the work presented in this article is focused to detect, discriminate interturn faults from ground faults, and to locate the faulty phase.

The study proposes a new automatic detection, classification of interturn, and ground faults from three-phase current signals of the IM. A three-stage stator fault diagnosis scheme for a three-phase IM is presented. The three-stage process is able to detect the fault, distinguish its type, and locate the faulty phase in the stator windings. The novelty of the algorithm lies in the simple features used in the time-frequency plane based on the variation around fault-related frequencies. Two stator winding faults, interturn and ground faults, are considered. The current signals for each stator winding condition are decomposed using the ST. In the first stage, the fault detection is performed with the help of variation of the chosen frequencies for a specified time. In the second stage, the type of fault is detected using zero-sequence current. Subsequently, in the last stage, the faulty phase is identified for both categories of faults.

TABLE I
HARMONICS PRESENT DUE TO STATOR WINDING INTERTURN FAULTS

$n\|k$	1	3	5
1	75/25 Hz	175/125 Hz	275/225 Hz
2	100/0 Hz	200/150 Hz	300/200 Hz
3	125/25 Hz	225/75 Hz	325/175 Hz

The article is organized into six sections. The first section is the introduction and the literature review of the stator winding faults. In Section II, a theoretical background of these faults is presented. In Section III, the details of the experimental setup have been provided. The fault diagnosis strategy is explained in Section IV. Results and discussions are presented in Section V. Section VI is the conclusion of the article.

III. THEORETICAL BACKGROUND

It has been reported in [29] that frequency components in the air-gap flux arising due to shorted stator turns are reflected in the stator current spectrum. Under stator turn-shorts, the air-gap magneto-motive force (MMF) distribution will change because of the modified current circulating through the shorted turns. These components in the air-gap flux generated around the fundamental component are given by the following equation:

$$f_a = \left[\frac{n}{p}(1-s) \pm k\right] f_m \tag{1}$$

where f_a are the turn-short-related frequency components, f_m is the supply frequency, p is the pair of poles, s is the per-unit slip, $n = 1, 2, 3, \ldots,$ and $k = 1, 3, 5, \ldots$

For different values of n and k, and with $s \approx 0$ for no-load operation, $f_m = 50$, and $p = 2$, the fault frequency components are calculated and given in Table I.

Due to voltage unbalances or other variations in the motor, frequency components with certain combinations of n and k are found to be useful for turn-fault diagnosis. The frequency components of 25 and 75 Hz cannot be utilized for fault diagnostic purposes as they also arise due to machine asymmetries. These components also arise due to motor eccentricity, and hence, they fail to discriminate shorted turns from air-gap eccentricity. They can also be produced due to shaft misalignment. The 100-Hz content may get affected by stator turn-faults as well the load variations. Thus, the frequency components of 25, 75, 50, and 100 Hz cannot be used for fault diagnostics. The frequencies 125 and 175 Hz have been reported to be varying with the turn-faults [29], and hence, they are used for the analysis of stator winding faults. These components are less affected by load variations and not affected by supply. Thus, these frequency components can be utilized for fault diagnosis. The other frequency component included for fault diagnosis is 225 Hz (as per Table I). Thus, 125, 175, and 225 Hz have been finalized for the purpose of stator winding fault diagnosis.

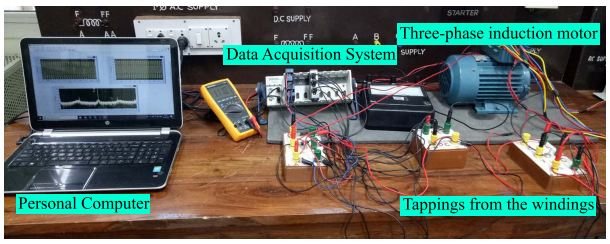

Fig. 1. Experimental set-up to record current signals for stator winding fault diagnosis.

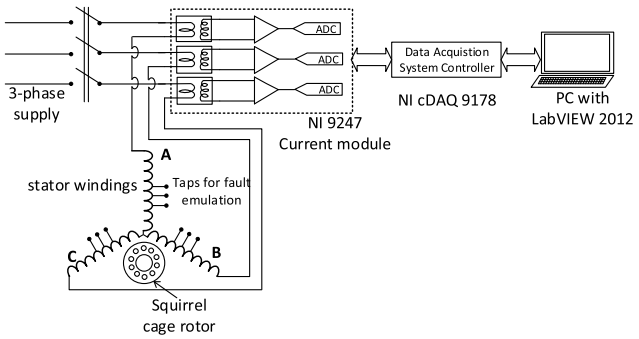

Fig. 2. Details of interconnections between the motor with taps from each winding, the data acquisition system, and the PC with LabVIEW 2012 for interface.

IV. Experimental Set-up

A three-phase IM rating 0.75 kW (1 HP), 415 V, 4-pole, 50 Hz, 2 A, and 1380 rpm has been used for the experimental study. The rotor is suspended with two bearings, that is, 6204 ZZ and 6203 ZZ. The winding faults taken into consideration are interturn and phase-to-ground fault. The stator current signals are recorded for different cases of these winding faults. For the reference, the current signals for a healthy motor (without fault) are taken also acquired. The signal acquisition is performed using a National Instruments-based data acquisition system comprising of NI 9178 chassis, NI 9247 current module, and an interfacing LabVIEW software with a personal computer. The current module is integrated in the chassis to connect with the motor. The module has a range from 0 to 50 A_{rms}, ± 147 A_{peak}, and withstands over 1250 A_{rms} for one cycle. It has up to 300 V_{rms} channel-to-earth and 480 V_{rms} Ch–Ch CAT III isolation with a maximum sampling rate of 50 kS/s/ch. The sampling frequency for the measurement is set to 6.4 kHz. The experimental hardware set-up used for the data acquisition is shown in Fig. 1. A schematic diagram of the experimental set up is shown in Fig. 2.

The faults are emulated in the motor by taking out connections from the windings and the core, shown in Fig. 3. For turn-faults, taps are provided on the three adjacent windings in each phase. These taps are located in the middle of each phase winding. The ground fault is emulated by a tap provided from the core of the motor. The details of the taps are given in Table II.

Since there are three taps available for each phase winding of the motor, three turn-shorts can be emulated for each phase. Thus, if A_1, A_2, and A_3 are three taps of phase A, then shorting of A_1–A_2, A_2–A_3, and A_1–A_3 are performed and the three-phase current signals are recorded. Thus, there are nine cases

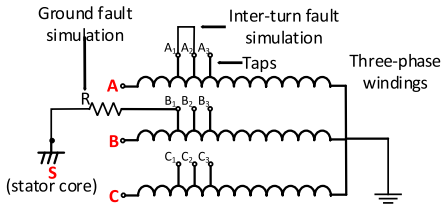

(a)

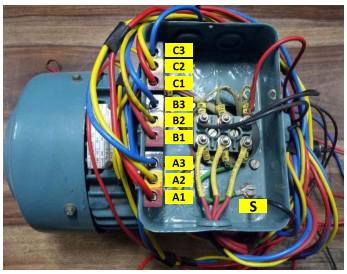

(b)

Fig. 3. (a) Schematic of the interturn and ground faults emulation in three-phase windings. (b) Top view of the motor showing connections from windings; A_1–A_3 for phase A, B_1–B_3 for phase B, C_1–C_3 for phase C, and S for stator core.

TABLE II
Details of the Emulated Stator Winding Faults

Fault Type	Details
Turn faults	Total taps on each phase: 3 Total phases: 3 Total taps for three-phases: 9 At a time, % turns shorted, 1.6% Total possible combinations of turn-shorts: 9
Ground faults	nine connections to ground with shorting resistor (R) R = 500 kΩ, 100 kΩ, 50 kΩ, 10 kΩ, 5 kΩ, 1 kΩ, 500 Ω

TABLE III
Total Current Data Set Recorded Under Various Motor Conditions

Condition	Phase-A	Phase B	Phase C	Total
Healthy	-	-	-	10
Turn-faults	18	18	18	54
Ground faults	63	63	63	189

of turn-shorts performed. For ground faults, each turn-tap is shorted with ground connection (S) taken out from stator core through a shorting resistor (R). In each experiment, data of all three-phase current signals with proper annotation of the location of the faulty phase are recorded. The details of the data set recorded for each condition of the motor are shown in Table III.

V. Stator Winding Fault Diagnosis

The stator current signals recorded for various states of stator windings (healthy, turn-faults, and ground faults) of

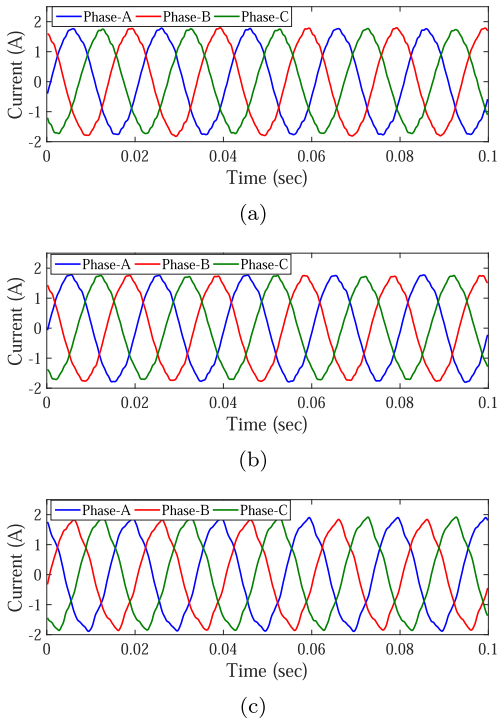

Fig. 4. Stator current signals for (a) healthy, (b) turn-fault, and (c) ground fault for a three-phase IM.

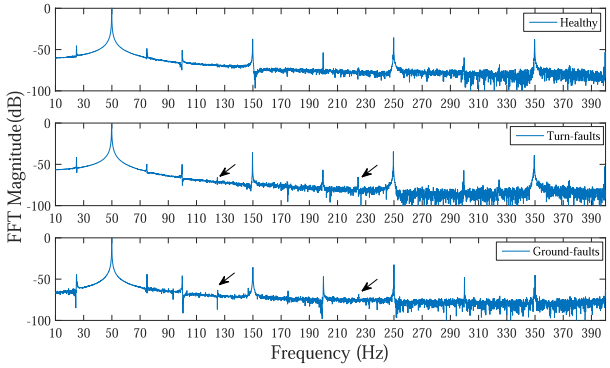

Fig. 5. Frequency spectrum (decibel) for healthy, turn-fault, and ground fault case for a range from 1 to 400 Hz.

a three-phase IM are shown in Fig. 4. Spectral analysis is performed using FFT to observe the variations of frequency content under different conditions of the motor. The power spectral density (PSD) of frequency spectrum is plotted in the stator current signals for all phase A under different stator conditions is shown in Fig. 5. The zoomed FFT for each turn-fault case in phase A is shown in Fig. 6(a) and ground faults in phase A using three shorting resistors are shown in Fig. 6(b). From both figures, it can be observed that the frequencies in (1) have low magnitudes peaks under fault cases only (highlighted).

The highlighted frequencies appear mostly in fault cases specially in turn-faults. The time variation of these frequencies can be useful for fault diagnostic purposes. Thus, a wider frequency range can be chosen. In ground faults, there are more peak other than those frequencies. Hence, the ST has

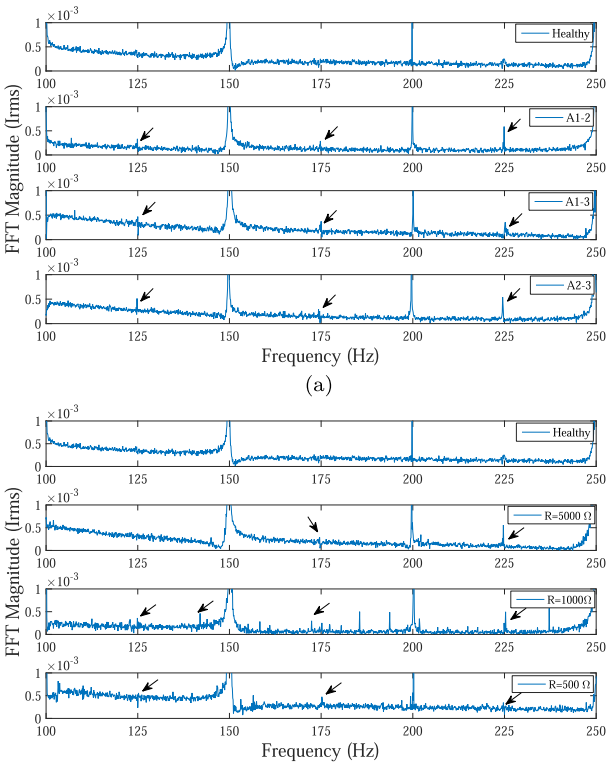

Fig. 6. FFT of stator current signals under healthy, and various cases of (a) turn-fault, and (b) ground faults conditions.

TABLE IV
DATA SET USED FOR DIFFERENT STAGES OF DIAGNOSIS

Stages	Detection of	Healthy	Turn-fault	Ground fault
Stage-1	fault	Y	Y	Y
Stage-2	type of fault	-	Y	Y
Stage-3	faulty phase	-	Y	Y

been proposed for using the time variation of these ranges of fault frequencies as features to be fed to classifiers to detect the faulty phase.

ST is implemented on the stator current signals recorded under various conditions of the stator winding. It decomposes each 1-D time-varying signal into time-varying frequency components obtained as a 2-D matrix, where the y-axis and x-axis represent frequency and time, respectively. The statistical properties of the 2-D ST matrix (row and column-wise) such as mean, maximum, standard deviation (SD), kurtosis, mean absolute deviation, skewness, energy, and entropy have been observed critically in the viewpoint of the features to be selected for fault diagnosis. SD for each frequency along the time axis is found to be the most promising feature for fault diagnosis. Subsequently, SD is used as a fault diagnostic parameter in the proposed algorithm. The proposed diagnostic method is carried out in the following stages.

Stage 1: Fault detection.

Stage 2: Identification of fault type (interturn and ground fault).

Stage 3: Detection of faulty phase.

In all stages, the utilization of collected data has been detailed in Table IV.

A. Fault Detection

For the detection of winding faults, the SD of each phase for the selected band of frequencies is determined. As stated in Section III, the chosen fault frequencies are 125, 175, and 225 Hz. A subband of frequencies with ±10 Hz around the chosen frequencies is selected to encompass the minor fluctuations. Thus, the subband frequency ranges are $\mathrm{Fr}_1 = [115-135]$ Hz for the fault frequency 125 Hz, $\mathrm{Fr}_2 = [165-185]$ Hz occupying 175 Hz, and $\mathrm{Fr}_3 = [215-225]$ Hz for 225 Hz. The SD of ST matrix is calculated for these subband frequency ranges. Fault index of each phase is computed to detect the fault as per the following equation:

$$\mathrm{FI}_1 = \sum_{i=1}^{3} \mathrm{std}(|S_i(\tau, f)|)_{\mathrm{Fr}_1,\mathrm{Fr}_2,\mathrm{Fr}_3} \tag{2}$$

where $S_i(\tau, f)$ is the ST matrix, $\mathrm{std}(|S_i(\tau, f)|$ is the SD of magnitude of the ST matrix for ith phase, and $i = 1, 2, 3$ represent all three phases. Thus, the fault index (FI_1) is the summation of the SD of magnitude matrices for the three phases. Using this index, the fault (turn-shorts or ground fault) can be detected by comparing it to a threshold.

B. Identification of Fault Type (Interturn and Ground Fault)

Postfault detection, the faults are classified into turn-faults and ground faults with the help of zero sequence current (ZSC). A fault index based on ZSC is defined by the following equation:

$$\mathrm{FI}_2 = \mathrm{std}(|I_0|) \tag{3}$$

where I_0 is the ZSC and is given as $I_0 = (I_a + I_b + I_c)/3$, and I_a, I_b, and I_c are the phase currents of winding A, B, and C, respectively. It has been observed that ground faults have much higher values when compared to turn-faults. Thus, this difference can be utilized to identify the nature of the fault.

C. Detection of Faulty Phase

Subsequent to fault type detection, the faulty phase is identified using the features of the ST matrices. Two separate SVM models, one for turn-faults and other for ground faults have been proposed. For both faults, the following steps are carried: feature extraction and classification using SVM.

1) Feature Extraction: The features are obtained from the SD of the magnitude of ST matrix for selected subband frequencies Fr_1, Fr_2, and Fr_3 for the phases A, B, and C current signals, respectively. These frequency ranges depend on the nature of faults, that is, turn-faults and ground faults. The process of feature formation for both type faults is detailed below.

a) Interturn faults: In the case of interturn faults, the frequency subbands are chosen as mentioned in the previous Section V-A. The feature is obtained as summation of the SD vector corresponding to a frequency subband which is given by the following equation:

$$\mathrm{fea1}_{i,j} = \sum_{\mathrm{Fr}_i^1}^{\mathrm{Fr}_i^2} \mathrm{std}(|S_i(\tau, f)|) \tag{4}$$

TABLE V
SELECTED FREQUENCY RANGES USEFUL FOR DETECTING THE FAULTY PHASE

Faulty Phases	Useful frequency ranges	Selected frequency ranges
Phase-A	300-350 Hz	280-350 Hz,
Phase-B	90-120 Hz, 280-350 Hz	100-120 Hz,
Phase-C	100-160 Hz, 190-240 Hz	190-240 Hz

where $\mathrm{std}(S_j(\tau, f))$ is the SD of magnitude of ST matrix for jth phase ($j = A, B, C$), Fr_i^1 and Fr_i^2 are the lower and upper bounds of the ith frequency range, where $i = 1,2, 3$ and these bounds are $\mathrm{Fr}_1^1 = 115$ Hz, $\mathrm{Fr}_1^2 = 135$ Hz, $\mathrm{Fr}_2^1 = 165$ Hz, $\mathrm{Fr}_2^2 = 185$ Hz, $\mathrm{Fr}_3^1 = 215$ Hz, and $\mathrm{Fr}_3^2 = 225$ Hz, and $\mathrm{fea1}_{i,j}$ is the feature of ith frequency range and jth phase. Thus, for all three phase current signals, there are nine features to represent the fault case.

b) Ground faults: The characteristics of ground faults may not precisely match with turn-faults, and hence, the same frequency subbands for turn-faults may not help in detecting faulty phase in the ground faults. To verify this, SD plots are critically observed (shown in Fig. 7) to find frequencies that can discriminate faulty phase under the ground faults. It can be observed that at the same frequency bands, the values of SD do not show any signature to detect a faulty phase. The underlying reason can be that the fault in one phase affects the currents in other phases, as neutral current flows back in the phases through the ground terminal. This causes a simultaneous effect on other phases also. This interphase effect does not change a small set of frequencies in the faulty phase, which leads to a wider range of frequencies getting affected due to the ground faults.

From Fig. 7, it is found that SD of phase A is high in frequency ranges 300–350 Hz under ground fault in phase A. In the case of the ground fault in phase B, the SD of phase B is higher for frequency ranges 90–120 Hz and 280–350 Hz. Similarly, phase C has higher values of SD in frequency ranges 100–160 Hz and 190–240 Hz for fault cases in phase C. The frequencies are highlighted in Fig. 7 and are listed in Table V.

The combination of these frequency ranges are chosen as the final frequencies for analysis which are $\mathrm{Fr}_1 = [280–350$ Hz], $\mathrm{Fr}_2 = [100–120$ Hz], and $\mathrm{Fr}_3 = [190–240$ Hz] as depicted in Table V. The features extracted within these frequency ranges for each phase are given by the following equation:

$$\mathrm{fea2}_{i,j} = \sum \mathrm{std}(|S_j(\tau, f)|)_{\mathrm{Fr}_1,\mathrm{Fr}_2,\mathrm{Fr}_3} \tag{5}$$

where i is the frequency subband, Fr_i, and $j = A, B, C$ is the jth phase. Thus, each feature $\mathrm{fea2}_{i,j}$ represents the summation of SD for ith frequency range and jth phase. Therefore, there are total nine features (three features for each phase) to represent a ground fault.

2) Classification Using SVM: Selection of relevant features is carried out using a features, $\sum C_r^n$ where $n = 9$ and $r = 2, 3, \ldots, 9$ which results in 502 combinations. Following steps are followed to select the relevant features.

Step 1: Initialize $n = 2$ and make the feature set with first n features.

Step 2: Compute the classification accuracy using SVM.

Step 3: Repeat the above procedure with a new set of features if the accuracy is less than 100% or all features are exhausted.

In this way, features providing the highest classification accuracy can be utilized for the purpose of faulty phase detection in both types of the winding faults.

3) Structure of SVM: SVM has been used for the classification of the faulty phase. Radial basis function is used as the kernel function on the basis of better performance when compared to other kernels such as linear, polynomial, and so on. This is a widely used kernel for the fault diagnosis strategies. The optimal values of the tuning parameters Gamma, γ, which is the width of the Gaussian function and cost, C, which sets soft-margin in the classifier are determined using k-fold cross-validation. Over the grid of γ and C, the training is performed and the pair of γ and C giving the highest average cross-validation accuracy is chosen. A heuristic approach is used to find the optimal features such that for every combination of features, the SVM model is trained and validated. With this, the optimal values of C and γ are obtained, which are later used to test the unknown/testing data set. The data set is split into 70:30 ratio for training and testing phases.

VI. Results and Discussion

The three-phase stator current signals are decomposed using ST to obtain complex 2-D matrices (ST matrices). These matrices present the magnitude and phase angle of various frequency components with respect to time. The analysis of these plots yields the algorithm for the detection and classification of the faults which has been detailed in the following stages below.

A. Stage 1

Fig. 8(a)–(c) shows the magnitude of SD over the selected frequency range 1–400 Hz for various nature of faults in phase A, phase B, and phase C, respectively. The critical observation of these plots would establish the fact that magnitude SDs of faulty cases are higher over certain frequency ranges compared to healthy cases. This difference in SD can be utilized to detect the fault in stator winding by computing fault index, FI_1 over a certain frequency range. Fig. 9 established the performance of the fault index. The mean value of the healthy reference can be set as a threshold.

B. Stage 2

The next stage of diagnosis is the detection of the type of fault, that is, turn-fault or ground fault. It is accomplished using fault index, FI_2 which is based on the SD of zero-sequence current. Fig. 10 illustrates the performance of the fault index computed over samples of both faults. A significant difference between the fault indices, FI_2 for turn-shorts and ground faults can be observed. The mid-value can be set as threshold to discriminate the fault type.

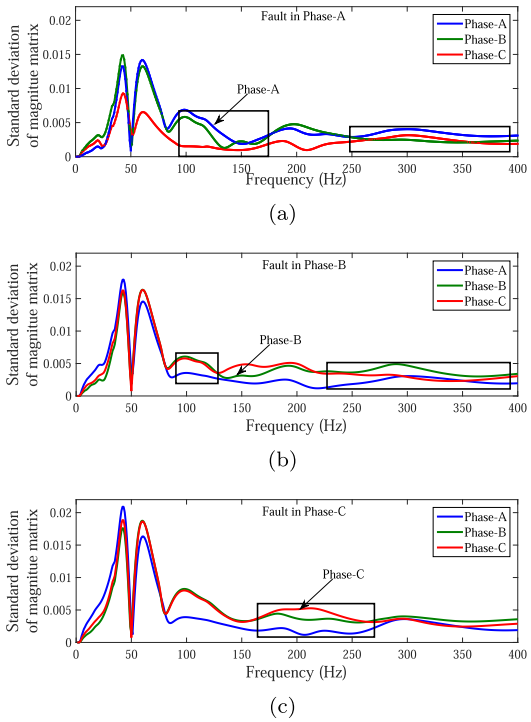

Fig. 7. SD of the ST matrix of stator current signals along frequency axis under ground fault conditions when the fault is in (a) phase A, (b) phase B, and (c) phase C windings.

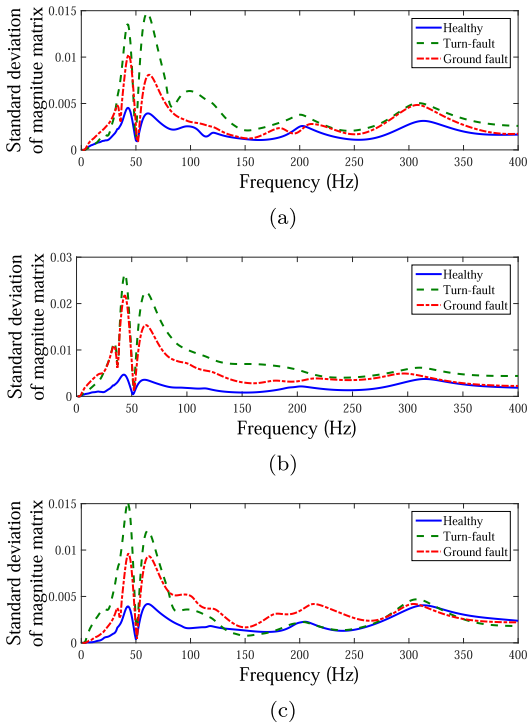

Fig. 8. SD of the ST matrix of stator current signals along the frequency axis for a healthy case, turn, and ground fault conditions in (a) phase A, (b) phase B, and (c) phase C.

C. Stage 3

The last stage of fault diagnosis is to identify the faulty phase for both types of faults. Two separate SVM models,

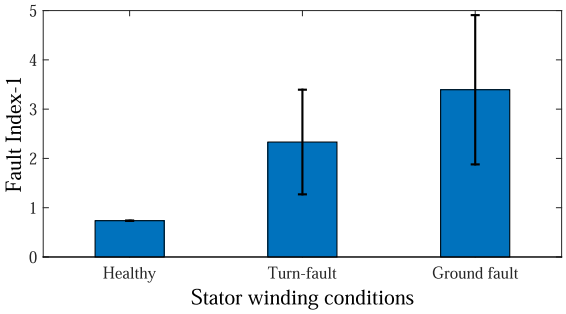

Fig. 9. Fault index for detecting faults in the stator windings.

TABLE VI

FEATURES SELECTED (WITH HIGHEST ACCURACY) FOR EACH SET OF COMBINATIONS FOR TURN-FAULTS

Number of features (n)	Selected features	Accuracy (%)
2	f_1,f_4	83.33
3	f_3,f_4,f_8	94.44
4	f_1,f_3,f_6,f_9	94.44
5	f_1,f_2,f_3,f_4,f_8	94.44
6	f_1,f_2,f_3,f_4,f_6,f_8	100

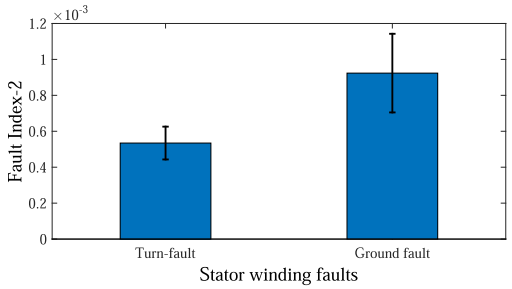

Fig. 10. Fault index for discriminating turn-faults and ground faults in stator windings.

TABLE VII

CONFUSION MATRIX FOR SVM-1

	A	B	C	Class Accuracy (%)	Overall Accuracy
A	6	0	0	100	100%
B	0	6	0	100	
C	0	0	6	100	

viz., SVM-1 and SVM-2 to find the faulty phase in the case of turn-faults and ground faults, respectively.

a) Turn-faults: Thirty-six out of 54 feature vectors (as described in Table III) are used to train SVM-1. The rest are utilized for testing the SVM. The cross-validation is performed with $k = 4$. Six features are found to be optimal during the training process presented in Table VI. The optimal values of C and γ are found as 2048 and 0.004, respectively. The accuracy of the SVM has been found to be 100%. The maximum accuracies obtained upto $n = 6$ feature combinations are plotted in Fig. 11.

The confusion matrix for this classification is provided in Table VII.

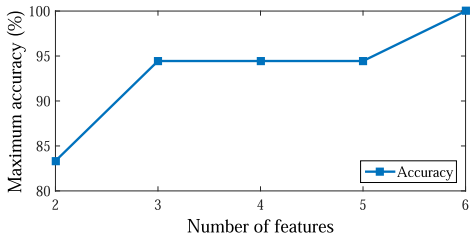

Fig. 11. Maximum accuracies for each set of feature combinations (n) for faulty phase detection in the case of turn-faults.

TABLE VIII

FEATURES SELECTED (WITH HIGHEST ACCURACY) FOR EACH SET OF COMBINATIONS FOR GROUND FAULTS

Number of features (n)	Selected features	Accuracy (%)
2	f_1,f_4	69.44
3	f_3,f_5,f_9	80.55
4	f_2,f_3,f_5,f_8	80.55
5	f_1,f_2,f_5,f_7,f_9	80.55
6	f_1,f_2,f_3,f_4,f_6,f_8	91.66
7	f_1,f_2,f_4,f_5,f_6,f_7,f_9	88.89
8	f_1,f_2,f_3,f_5,f_6,f_7,f_8,f_9	77.78
9	ALL	77.78

TABLE IX

CONFUSION MATRIX FOR SVM-2

	A	B	C	Class Accuracy (%)	Overall Accuracy
A	12	0	0	100	91.66%
B	1	10	1	83.33	
C	0	0	12	100	

b) Ground faults: A total of 153 out of 189 feature vectors are used for the training of SVM-2. The remaining 36 vectors are used for testing purposes. The cross-validation is performed with $k = 10$. Six features are found to give the highest accuracy of detection of the faulty phase. Fig. 12 shows the maximum accuracy obtained for all combinations of features ($n = 1, 2, 3, \ldots, 9$) to classify under three phases. With six features, a classification accuracy of 91.66% is obtained with $C = 64$ and $\gamma = 0.5$. Table VIII shows the features giving the highest accuracy for each set of n. Table IX shows the confusion matrix for the classification giving the highest accuracy.

Hence, with these features, the faulty phase can be identified in the case of ground faults. With this step, a complete algorithm is established which first detects the presence of fault and its type, followed by detection of faulty phase in both cases using ML approach. The flowchart of the fault detection algorithm for stator winding faults is shown in Fig. 13.

This work contributes in terms of proposing a single algorithm which has ability to detect the stator winding fault, its nature, and its location (faulty phase) to a fair accuracy. However, the proposed algorithm requires validation in terms of changes in 1) capacity, 2) brand, 3) physical location of the fault, 4) variations in supply, and 5) variations in load.

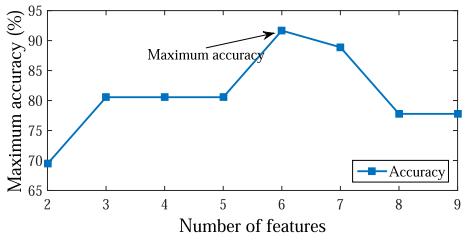

Fig. 12. Maximum accuracies for each set of feature combinations (n) for faulty phase detection in case of ground faults.

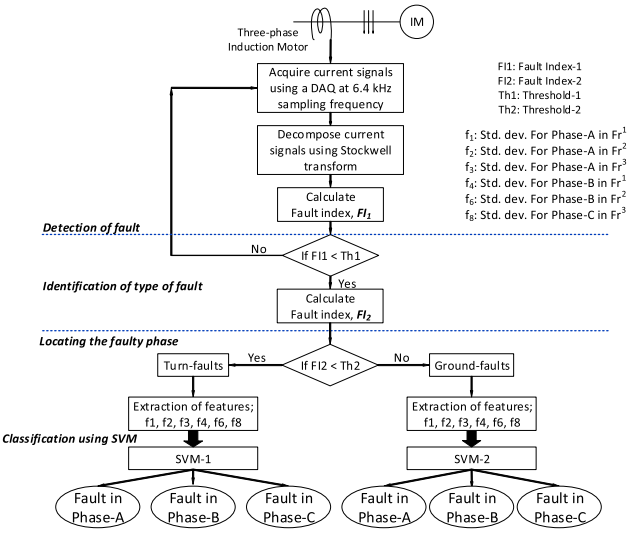

Fig. 13. Flowchart of the fault diagnosis strategy for stator winding faults.

VII. Conclusion

In this work, a fault diagnosis scheme for detection, classification, and location of stator winding faults in a three-phase IM is proposed which makes use of ST decomposition of stator currents. It has been observed that the SD of magnitude of ST matrix is suitable for fault diagnosis purposes. The first stage of fault diagnosis utilizes the fault index defined based on this SD to detect the fault. Another fault index based on ZSC is used to discriminate ground faults from turn-faults. Two SVM models have been trained to detect faulty phases for turn-faults and ground faults by extracting the range of various features for different phases. An accuracy of 100% and 91.66% is obtained for turn-fault and ground faults, respectively.

References

[1] Motor Reliability Working Group, Power Systems Engineering Sub Committee, Industrial and Commercial Power System Department, and IEEE Industry Applications Society, "Report of large motor reliability survey of industrial and commercial installations: Part 1," *IEEE Trans. Ind. Appl.*, vol. IA-23, no. 1, pp. 153–158, 1987.

[2] O. V. Thorsen and M. Dalva, "A survey of faults on induction motors in offshore oil industry, petrochemical industry, gas terminals, and oil refineries," *IEEE Trans. Ind. Appl.*, vol. 31, no. 5, pp. 1186–1196, Sep. 1995.

[3] S. Grubic, J. M. Aller, B. Lu, and T. G. Habetler, "A survey on testing and monitoring methods for stator insulation systems of low-voltage induction machines focusing on turn insulation problems," *IEEE Trans. Ind. Electron.*, vol. 55, no. 12, pp. 4127–4136, Dec. 2008.

[4] A. Siddique, G. S. Yadava, and B. Singh, "A review of stator fault monitoring techniques of induction motors," *IEEE Trans. Energy Convers.*, vol. 20, no. 1, pp. 106–114, Mar. 2005.

[5] R. Sharifi and M. Ebrahimi, "Detection of stator winding faults in induction motors using three-phase current monitoring," *ISA Trans.*, vol. 50, no. 1, pp. 14–20, Jan. 2011.

[6] P. V. J. Rodríguez and A. Arkkio, "Detection of stator winding fault in induction motor using fuzzy logic," *Appl. Soft Comput.*, vol. 8, no. 2, pp. 1112–1120, Mar. 2008.

[7] V. Nguyen *et al.*, "A method for incipient interturn fault detection and severity estimation of induction motors under inherent asymmetry and voltage imbalance," *IEEE Trans. Transport. Electrific.*, vol. 3, no. 3, pp. 703–715, Sep. 2017.

[8] S. Das, P. Purkait, C. Koley, and S. Chakravorti, "Performance of a load-immune classifier for robust identification of minor faults in induction motor stator winding," *IEEE Trans. Dielectr. Electr. Insul.*, vol. 21, no. 1, pp. 33–44, Feb. 2014.

[9] D. G. Dorrell and K. Makhoba, "Detection of inter-turn stator faults in induction motors using short-term averaging of forward and backward rotating stator current phasors for fast prognostics," *IEEE Trans. Magn.*, vol. 53, no. 11, pp. 1–7, Nov. 2017.

[10] M. E. H. Benbouzid, "A review of induction motors signature analysis as a medium for faults detection," *IEEE Trans. Ind. Electron.*, vol. 47, no. 5, pp. 984–993, 2000.

[11] P. Nussbaumer, M. A. Vogelsberger, and T. M. Wolbank, "Induction machine insulation health state monitoring based on online switching transient exploitation," *IEEE Trans. Ind. Electron.*, vol. 62, no. 3, pp. 1835–1845, Mar. 2015.

[12] Y. Liu and A. M. Bazzi, "A review and comparison of fault detection and diagnosis methods for squirrel-cage induction motors: State of the art," *ISA Trans.*, vol. 70, pp. 400–409, Sep. 2017.

[13] N. R. Devi, D. V. S. S. Siva Sarma, and P. V. Ramana Rao, "Diagnosis and classification of stator winding insulation faults on a three-phase induction motor using wavelet and MNN," *IEEE Trans. Dielectr. Electr. Insul.*, vol. 23, no. 5, pp. 2543–2555, Oct. 2016.

[14] J. Seshadrinath, B. Singh, and B. K. Panigrahi, "Single-turn fault detection in induction machine using complex-wavelet-based method," *IEEE Trans. Ind. Appl.*, vol. 48, no. 6, pp. 1846–1854, Nov. 2012.

[15] J. Seshadrinath, B. Singh, and B. K. Panigrahi, "Incipient interturn fault diagnosis in induction machines using an analytic wavelet-based optimized Bayesian inference," *IEEE Trans. Neural Netw. Learn. Syst.*, vol. 25, no. 5, pp. 990–1001, May 2014.

[16] J. Seshadrinath, B. Singh, and B. K. Panigrahi, "Incipient turn fault detection and condition monitoring of induction machine using analytical wavelet transform," *IEEE Trans. Ind. Appl.*, vol. 50, no. 3, pp. 2235–2242, May 2014.

[17] A. Sapena-Bano, M. Pineda-Sanchez, R. Puche-Panadero, J. Martinez-Roman, and D. Matic, "Fault diagnosis of rotating electrical machines in transient regime using a single stator current's FFT," *IEEE Trans. Instrum. Meas.*, vol. 64, no. 11, pp. 3137–3146, Nov. 2015.

[18] D. Dou and S. Zhou, "Comparison of four direct classification methods for intelligent fault diagnosis of rotating machinery," *Appl. Soft Comput.*, vol. 46, pp. 459–468, Sep. 2016.

[19] R. Liu, B. Yang, E. Zio, and X. Chen, "Artificial intelligence for fault diagnosis of rotating machinery: A review," *Mech. Syst. Signal Process.*, vol. 108, pp. 33–47, Aug. 2018.

[20] C. T. Kowalski and T. Orlowska-Kowalska, "Neural networks application for induction motor faults diagnosis," *Math. Comput. Simul.*, vol. 63, nos. 3–5, pp. 435–448, Nov. 2003.

[21] V. N. Ghate and S. V. Dudul, "Optimal MLP neural network classifier for fault detection of three phase induction motor," *Expert Syst. Appl.*, vol. 37, no. 4, pp. 3468–3481, Apr. 2010.

[22] M. S. Ballal, Z. J. Khan, H. M. Suryawanshi, and R. L. Sonolikar, "Adaptive neural fuzzy inference system for the detection of inter-turn insulation and bearing wear faults in induction motor," *IEEE Trans. Ind. Electron.*, vol. 54, no. 1, pp. 250–258, Feb. 2007.

[23] M. F. S. V. D'Angelo, R. M. Palhares, R. H. C. Takahashi, R. H. Loschi, L. M. R. Baccarini, and W. M. Caminhas, "Incipient fault detection in induction machine stator-winding using a fuzzy-Bayesian change point detection approach," *Appl. Soft Comput.*, vol. 11, no. 1, pp. 179–192, Jan. 2011.

[24] N. Rama Devi, S. Abdul Gafoor, and P. V. R. Rao, "Wavelet ANN based stator internal faults protection scheme for 3-phase induction motor," in *Proc. 5th IEEE Conf. Ind. Electron. Appl.*, Jun. 2010, pp. 1457–1461.

[25] M. Z. Ali, M. N. S. K. Shabbir, X. Liang, Y. Zhang, and T. Hu, "Machine learning-based fault diagnosis for Single- and multi-faults in induction motors using measured stator currents and vibration signals," *IEEE Trans. Ind. Appl.*, vol. 55, no. 3, pp. 2378–2391, May 2019.

[26] S. Haroun, A. N. Seghir, and S. Touati, "Multiple features extraction and selection for detection and classification of stator winding faults," *IET Electr. Power Appl.*, vol. 12, no. 3, pp. 339–346, Mar. 2018.

[27] G. H. Bazan, P. R. Scalassara, W. Endo, A. Goedtel, W. F. Godoy, and R. H. C. Palácios, "Stator fault analysis of three-phase induction motors using information measures and artificial neural networks," *Electr. Power Syst. Res.*, vol. 143, pp. 347–356, Feb. 2017.

[28] G. H. Bazan, P. R. Scalassara, W. Endo, A. Goedtel, R. H. C. Palacios, and W. F. Godoy, "Stator short-circuit diagnosis in induction motors using mutual information and intelligent systems," *IEEE Trans. Ind. Electron.*, vol. 66, no. 4, pp. 3237–3246, Apr. 2019.

[29] W. T. Thomson and D. Morrison, "On-line diagnosis of stator shorted turns in mains and inverter fed low voltage induction motors," in *Proc. Int. Conf. Power Electron., Mach. Drives*. Santa Fe, NM, USA: IET, 2002, pp. 122–127.

[30] W. Yang, C. Little, and R. Court, "S-transform and its contribution to wind turbine condition monitoring," *Renew. Energy*, vol. 62, pp. 137–146, Feb. 2014.

[31] M. Singh and A. G. Shaik, "Faulty bearing detection, classification and location in a three-phase induction motor based on stockwell transform and support vector machine," *Measurement*, vol. 131, pp. 524–533, Jan. 2019.

Megha Singh (Student Member, IEEE) received the B.Tech. degree in electronics instrumentation and control engineering from Rajasthan Technical University, Kota, India, in 2010, the M.Tech. degree in electrical engineering from the M.B.M. Engineering College, Jodhpur, India, in 2013, and the Ph.D. degree from IIT Jodhpur, Jodhpur, India, in 2020, with a focus on fault diagnosis of three-phase induction motor.

She is currently working with General Electric Power Conversion, Chennai, India. Her research interests include electrical machine fault diagnosis, signal processing, machine learning, and data analysis.

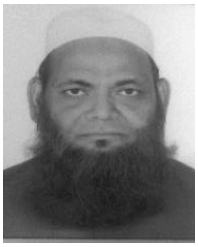

Abdul Gafoor Shaik received the B.Tech. degree in electrical engineering from the Regional Engineering College (REC) Warangal, Hanamkonda, India, in 1989, the M.Tech. degree in power systems from IIT Kanpur, Kanpur, India, in 1991, and the Ph.D. degree in power system protection from National Institute of Technology (NIT) Warangal, Hanamkonda, India, in 2008.

He is currently an Associate Professor with the Department of Electrical Engineering, IIT Jodhpur, Jodhpur, India. His research interests include power system studies, protection, distribution networks, protection with distribution generation (DG) penetration and power quality assessment and mitigation, and condition monitoring of electrical equipment.